Available online at www.sciencedirect.com
SCIENCE DIRECT®
Journal of Membrane Science 237 (2004) 145–161
journal of MEMBRANE SCIENCE
www.elsevier.com/locate/memsci

A comparison of physical properties and fuel cell performance of Nafion and zirconium phosphate/Nafion composite membranes

Chris Yang [a,1], S. Srinivasan [b], A.B. Bocarsly [b], S. Tulyani [c], J.B. Benziger [c,*]

[a] *Department of Mechanical and Aerospace Engineering, Princeton University, Princeton, NJ 08544, USA*
[b] *Chemistry Department, Princeton University, Princeton, NJ 08544, USA*
[c] *Department of Chemical Engineering, Princeton University, Princeton, NJ 08544, USA*

Received 12 December 2003; received in revised form 10 March 2004; accepted 11 March 2004

Abstract

The physiochemical properties of Nafion 115 and a composite Nafion 115/zirconium phosphate (∼25 wt.%) membranes are compared. The composite membrane takes up more water than Nafion at the same water activity. However, the proton conductivity of the composite membrane is slightly less than that for Nafion 115. Small angle X-ray scattering shows that the hydrophilic phase domains in the composite membrane are spaced further apart than in Nafion 115, and the composite membrane shows less restructuring with water uptake. Despite the lower proton conductivity of the composite membranes they display better fuel cell performance than Nafion 115 when the fuel cell is operated at reduced humidity conditions. It is suggested that the composite membrane has a greater rigidity that accounts for its improved fuel cell performance.

Keywords: Composite membranes; Water sorption and diffusion; Fuel cells

1. Introduction

Polymer electrolyte fuel cells based upon perfluorinated membranes have typically been operated in a temperature range between approximately 50 and 90 °C [1–3]. This temperature range is a compromise between competing factors. Increasing the operating temperature above room temperature will improve the electrode kinetics of the oxygen reduction reaction [4,5]. The upper limit of temperature results from the difficulty in maintaining membrane water content at temperatures at or above 100 °C. In addition, temperatures above the polymer glass transition temperature (∼110 °C for protonated Nafion) can cause polymer chain rearrangements, which can lead to structural changes in the membrane and lower the membrane stability, performance, and lifetime [6–8].

Polymer membranes able to operate above 120 °C could benefit from both enhanced carbon monoxide (CO) tolerance and improved heat removal [9]. The most significant barrier to running a polymer electrolyte fuel cell at elevated temperatures is maintaining the proton conductivity of the membrane. Higher temperature increases the water vapor pressure required to keep a given amount of water in the membrane, thereby increasing the likelihood that water loss will occur and significantly reduce proton conductivity. The conductivity of a dry membrane is several orders of magnitude lower than a fully saturated membrane. A number of alternative strategies have been investigated to maintain membrane conductivity in a dehydrating environment (i.e. elevated temperature and reduced relative humidity). Two recent reviews summarize these strategies well [5,10].

The addition of an inorganic material into a polymer membrane can alter and improve physical and chemical polymer properties of interest (such as elastic modulus, proton conductivity, solvent permeation rate, tensile strength, hydrophilicity, and glass transition temperature) while retaining its important polymer properties to enable operation in the fuel cell. A number of investigators have examined composite membranes for use in polymer electrolyte fuel cells [5,10–25]. The hydration properties of membranes are key characteristics that can influence fuel cell performance. The composite membranes may improve the water-retention properties of these membranes under low humidity

* Corresponding author. Tel.: +1-609-2585416; fax: +1-609-2580211.
E-mail address: benziger@princeton.edu (J.B. Benziger).
[1] Current address: University of California Davis, Davis, CA, USA.

0376-7388/$ – see front matter © 2004 Elsevier B.V. All rights reserved.
doi:10.1016/j.memsci.2004.03.009

conditions. The conductivity of perfluorinated sulfonic acid membranes vary over many orders of magnitude depending upon the water activity and temperature. Models for proton conduction in Nafion have been proposed that provide a good semi-quantitative prediction of the conductivity at water activities greater than 0.2 [26,27]. However, very little has been done to characterize the conductivity of Nafion above 100 °C or to characterize the proton conductivity in composite membranes [19]. We have compared water uptake, proton conductivity, microstructure morphology and fuel cell performance of Nafion and Nafion/zirconium phosphate composite membranes as functions of temperature (80–140 °C) and water activity. We also tested the performance of composite polymer/inorganic membranes (Nafion/zirconium phosphate) in fuel cells at elevated temperatures. In this paper we compare the chemical and physical properties of Nafion membranes and Nafion/zirconium phosphate composite membranes to elucidate the role of zirconium phosphate in altering the membrane performance in PEM fuel cells.

2. Experimental

2.1. Membrane preparation

Nafion/zirconium phosphate (Nafion/ZP) composite membranes were prepared using Nafion® 115 films (DuPont) as the base material. To obtain uniform high-purity Nafion membranes as starting material, the membranes were cleaned with a standard treatment procedure: (i) boiling in 3% hydrogen peroxide for 1 h to oxidize organic impurities; (ii) rinsing with boiling water for several hours; (iii) boiling in 1 M sulfuric acid for 1 h to remove any metallic/ionic impurities; and (iv) rinsing again in boiling water to remove any excess acid.

Zirconium hydrogen phosphate ($Zr(HPO_4)_2{\cdot}H_2O$) was the desired additive to Nafion-based membranes because of its attributes, including: (i) it has moderate proton conductivity when humidified ($\sim 10^{-3}$ S/cm) [28–37]; (ii) it is a Brønsted acid with the ability to donate protons; (iii) it is thermally stable to temperatures above 180 °C; (iv) it is hygroscopic and hydrophilic; and (v) it is easily synthesized in a manner that is compatible with the chemical and physical limits of the polymer membrane [24]. In practice the zirconium phosphate phase may vary from amorphous to crystalline; the proton conductivity of zirconium phosphate can vary from 10^{-7} to 10^{-3} S/cm depending on the phase composition, structure and hydration state.

Zirconium phosphate was incorporated into Nafion using the procedure first described by Grot and Rajendran [14]. The synthesis involves the reaction of a solution of Zr^{4+} ions with phosphoric acid (H_3PO_4) leading to the precipitation of the insoluble zirconium phosphate. To accomplish this synthesis within the membrane, the procedure takes advantage of the fact that Nafion and other perfluorosulfonic acid ionomers are ion-exchange membranes. The protons are exchanged with zirconium ions and the zirconium ions are subsequently reacted in place with phosphoric acid.

First, the membranes were weighed in the dry state, and then swollen in a boiling methanol–water solution (1:1 (v/v)) to expand the membrane and facilitate ionic diffusion. The membranes were then dipped into a 1 M solution of zirconyl chloride, $ZrOCl_2$ (Aldrich) for several hours at 80 °C. The $ZrOCl_2$ solution diffuses into the membrane and the excess of Zr^{4+} ions within the membrane leads to an exchange with sulfonic acid protons in the membrane. The membranes were then rinsed in cold water to remove the zirconyl chloride solution from the surface and then immersed in 1 M phosphoric acid (H_3PO_4) overnight at 80 °C. The phosphoric acid has two purposes: (i) it reacts with the Zr^{4+} ions to precipitate insoluble zirconium hydrogen phosphate in situ, and (ii) the acidic solution can re-protonate the sulfonate anions to regenerate the acidity of the membrane. The membranes were then repeatedly boiled for several hours in distilled water to remove any excess acid and $ZrOCl_2$ solution. After drying, membrane weight and thickness increased about 25 and 30%, respectively, as compared with the unmodified membrane.

2.2. Physical/chemical characterization

The cross-sections of several Nafion and composite Nafion/zirconium phosphate membranes were analyzed using a Cameca SX50 experimental microprobe to determine the presence and distribution of zirconium phosphate. Micrographs revealed that the control Nafion contains negligible quantities of Zr and P, while the composite membranes have Zr and P uniformly distributed throughout the cross-section.

Powder X-ray diffraction (XRD) patterns for the composite membranes were obtained at CNR-ITAE using a Philips X-Pert 3710 X-ray diffractometer using Cu Kα source operating at 40 kV and 30 mA.

Ion-exchange capacity (IEC) was determined by an exchange of acidic protons with Na^+ ions in solution [38,39]. The membranes were dried and weighed and then placed in a 1 M NaCl solution at 80 °C overnight to exchange Na^+ ions with H^+. A large excess of Na^+ ions in the solution ensured nearly complete ion exchange. The membranes were removed from solution and the solution was titrated to the phenolphthalein end point with 0.1 M NaOH solution to determine the quantity of exchanged H^+ ions. The ion-exchange capacity and equivalent weight (grams of polymer per mole of H^+) were calculated using the dry weight of the polymer and the quantity of exchanged protons.

2.3. Water uptake and membrane conductivity

The water uptake and the proton conductivity measurements were carried out in a temperature-controlled barometric sorption vessel. The barometric sorption appa-

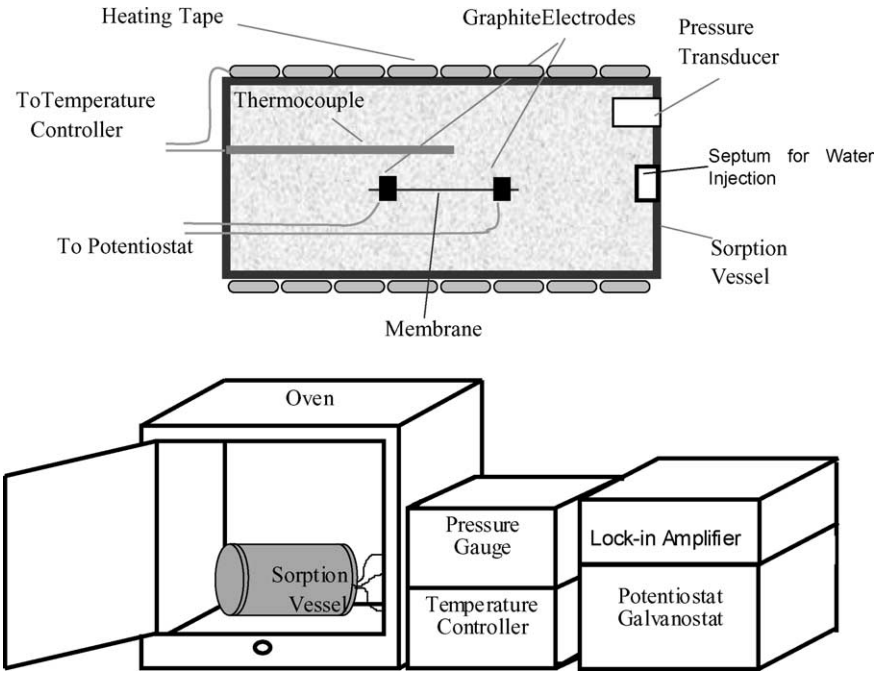

Fig. 1. Schematic of the barometric sorption apparatus for measuring water uptake and conductivity of membranes. A membrane sample was mounted between two graphite electrodes inside the temperature-controlled pressure vessel. The sorption vessel is shown placed in an oven to maintain a uniform temperature everywhere and avoid temperature gradients inside the sorption vessel.

ratus, shown in Fig. 1, is based on a design described by Miyake et al. [19].

The sorption vessel volume, V, is 430 mL. It is equipped with an Omega pressure transducer, copper and thermocouple wire feedthroughs, and Swagelok® fittings with a septum for water injection. The unconstrained dry membrane is placed within the sorption vessel, which is evacuated at the measurement temperature (80–140 °C) for over an hour to dry the membrane and remove any residual water from the vessel. Water is injected into the vessel through the septum using a microliter syringe.

At temperatures between 80 and 140 °C, the small mass of water, m_{H_2O}, that is injected (typically 5–50 μL) evaporates quickly and increases the pressure in the vessel. Using the ideal gas law, the expected pressure, P_{exp}, associated with the vaporization of the injected water can be calculated:

$$P_{exp} = \frac{m_{H_2O} RT}{18V} \quad (1)$$

$$N_{H_2O} = \frac{V(P_{exp} - P_{act})}{RT} \quad (2)$$

The difference between the expected pressure and the actual measured pressure, P_{act}, is attributed to water uptake by the membrane and the number of moles of water in the membrane, N_{H_2O}, can be calculated. The number of moles of sulfonic acid in the membrane is calculated from the dry weight of polymer in the membrane, m_{mem}, and equivalent weight, EW:

$$N_{SO^{3-}} = \frac{m_{mem}}{EW} \quad (3)$$

Finally the membrane water content parameter, λ, the number of moles of water per mole of sulfonate, can be calculated:

$$\lambda = \frac{N_{H_2O}}{N_{SO^{3-}}} \quad (4)$$

After allowing at least 30 min for membrane equilibration with the vapor phase, another small quantity of water is injected and the pressure is measured again. This procedure is repeated until no pressure rise is detected with the water injection, which indicates that the saturation vapor pressure, P_{sat}, is reached.

Within the sorption vessel, the membrane conductivity was measured using an ac impedance technique to isolate the bulk membrane resistance from other resistance factors.

The conductivity of the perfluorinated sulfonic acid membranes is measured along the longitudinal direction (in plane) of the membrane. A small piece of the membrane is placed between a set of graphite blocking electrodes spaced 1 cm apart. The graphite electrodes are connected through the vacuum feedthroughs on the sorption vessel to the measurement equipment. The two-probe frequency-dependent impedance measurement was carried out on a Princeton Applied Research (PAR) Model 398 Electrochemical Impedance System, consisting of a potentiostat/galvanostat Model 273A and a lock-in amplifier Model 5210 which are connected to a PC running Electrochemical Impedance Software (EIS). The applied signal is a single sine wave of 5 mV with frequencies varying between 10^5 and 10 Hz. The membrane resistance was taken from the zero frequency limit of the impedance.

2.4. Small angle X-ray scattering (SAXS)

2.4.1. SAXS sample preparation

Nafion membranes and Nafion/zirconium phosphate composite membranes were used after the cleaning treatment procedure described above. Before each set of runs, the membrane was placed in boiling de-ionized water to ensure full hydration. The membrane was then placed in a viton-sealed copper sample cell with mica windows. The cell was opened and the membrane was slowly dehydrated between runs. Membrane water content, λ, was determined gravimetrically.

2.4.2. SAXS data collection and analysis

The sample cell was placed in the path of the X-ray beam. Membrane water loss during the data collection was minimized by filling the flight tube with helium rather than a vacuum. The 1.5418 Å Cu Kα X-rays were generated by a Philips XRG-3000 sealed tube generator source. The beam was slit collimated and the scattering was detected by an Anton-Paar compact Kratky camera equipped with a Braun OED-50M detector. Samples were typically run at room temperature for 10 min. Background beam scattering, sample transmittance, and detector response were corrected for in the data analysis. The data reduction and desmearing procedures are described in detail by Register and Bell [40]. The invariant scattering intensity (q^2I) is plotted as a function of scattering angle or distance and the Bragg spacing is determined by the location of the peak in scattering intensity.

2.5. Water transport

The water flux through different membranes was measured at 80 °C. Liquid water was fed to the one side of the membrane and a dry gas was flowed to the opposite side. Nafion 115, Nafion 117, and Nafion 115/zirconium phosphate membranes were prepared as previously described. Each of these membranes was hot-pressed at 135 °C without electrodes, between sealing gaskets for 2 min at 10 kN (1 metric ton).

The membrane was placed in a 5 cm^2 fuel cell housing with triple-pass serpentine flow fields and heated to 80 °C. Liquid water was passed through the flow field on one side of the membrane and a dry N_2 stream was passed through the other side. The water vapor in the nitrogen outlet was condensed in a cold trap at 0 °C and collected in a graduated cylinder. The water flux through the membrane was determined as a function of the nitrogen flow rate to extrapolate to zero gas side mass transfer resistance.

2.6. Fuel cell tests

2.6.1. Membrane electrode assembly (MEA) preparation

Commercial gas-diffusion electrodes (20% Pt-on-carbon, 0.4 mg Pt/cm^2, purchased from E-TEK) were brushed with 5 wt.% solubilized Nafion (Aldrich) to impregnate the active layer (0.6 mg/cm^2) and then dried at 80 °C for 1 h. The geometrical area of the electrodes was 5 cm^2. A membrane was sandwiched between two electrodes and gas sealing gaskets, and the membrane electrode assembly was then pressed for 2 min at 135 °C at 20 MPa using a Carver hot press.

2.6.2. Single cell test fixture and performance evaluation

The MEAs, coupled with gas-sealing gaskets, were placed in a single cell test station. H_2 and O_2 gases were fed to the single cell at 100 sccm. The gases were bubbled through water in temperature-controlled stainless steel bottles to humidify the feeds prior to entry to the fuel cell. The baseline test was total pressure of 1 bar, cell temperature of 80 °C, and the humidifier bottles at $T_{anode} = 90$ °C and $T_{cathode} = 88$ °C, respectively. Performance evaluations were carried out at 120–140 °C with backpressure regulators at the effluents from the fuel cell fixed at 3 bar. The temperatures of the humidifier bottles were varied to alter the water vapor pressure (water activity) of the feed. The maximum temperature of the humidifier bottles was 130 °C, corresponding to an equilibrium water vapor pressure of 2.65 bar (the actual water vapor pressure is less due to finite mass transport rates in the bubblers). H_2 and O_2 partial pressures were always the difference between the total pressure of 3 bar and the water vapor pressure.

The fuel cell performance was characterized by current–voltage measurements (polarization curves). These were recorded at 80 °C and atmospheric pressure as well as in the range of temperatures between 80 and 140 °C, and total pressure of 3 bar pressure. The fuel cell was preconditioned by operating at 0.3 V and high current density prior to the performance measurement.

Current–voltage measurements were obtained by connecting the fuel cell to a load resistance (either carbon film resistors or an electronic Amrel load), and allowing the current and voltage output of the single cell to settle to fixed values (~5–20 s). After the values of current and voltage were recorded, a new load condition was used and the single cell output was recorded. The measurements were made starting at open circuit (zero current) and increasing current with each subsequent load condition. Because the entire current–potential curve for a given temperature/humidification condition is obtained in a couple of minutes, it is assumed that the membranes have constant water content throughout the measurement.

3. Results

3.1. Physical/chemical characterization

Table 1 compares the density change and ion-exchange capacity for Nafion 115 and the Nafion/zirconium phosphate composite membrane. The membranes were dried at 80 °C in vacuum for >4 h prior to the measurements. The density of the composite membrane is significantly lower than expected

Table 1
Physical characteristics of Nafion and Nafion/zirconium hydrogen phosphate composite membranes

Membrane	Thickness (μm)	Density (g/cm^3)	IEC (μeq/g)	EW (g/mol H$^+$)
Nafion 115	130	2.0	996	1004
Nafion/zirconium phosphate (25%)	170	1.6	1464	683

based upon the density of Nafion and zirconium phosphate (2.1 g/cm^3). The low density of the composite membrane suggests it has void volume. Residual water associated with zirconium phosphate which is not driven off at 80 °C is ignored.

XRD patterns were obtained for the composite membrane in varying states of hydration: (i) a fully hydrated membrane (equilibrated with liquid water), (ii) a partially hydrated membrane, and (iii) a thoroughly dried membrane. The hydrated membrane shows only one weak peak ca. 2.64 Å, whereas the well-dried membrane shows several sharp, well-defined peaks (Fig. 2). Diffraction maxima for the composite membrane may be attributed to Teflon-like domains of Nafion (5.2 and 2.3 Å) [41], and others that are attributed to the presence of zirconium phosphate phases (4.5, 3.73, 2.64, and 1.7 Å). Some of the zirconium phosphate peaks match up with typical peaks found in alpha zirconium hydrogen phosphate hemihydrate (4.46 and 3.54 Å) [42]. The X-ray patterns are not very sharp, and water uptake by the membrane disrupts the crystalline microstructure of the Nafion. It is likely that the membrane swelling due to water uptake influences the crystalline packing of polymer chains as well as the structure of the zirconium phases.

Diffraction peak width was used to estimate the particle size of the zirconium phosphate by using the Debye-Sherrer formula with Warren correction for instrumental effects. In the fully dried membrane the zirconium phosphate particles are estimated to be 11 ± 1 nm in size.

Table 2
Saturation water uptake by Nafion and Nafion/ZP composite membranes

Membrane treatment	Liquid water uptake (25 °C)		Water vapor uptake (80 °C)	
	wt.%	λ (H_2O/SO_3H)	wt.%	λ (H_2O/SO_3H)
Nafion 115	41	25	18	11
Nafion 115/ZP (25%)	33	25	25	19

The ion-exchange capacity and equivalent weight (grams of polymer per mole of H$^+$) were calculated using the dry weight of the polymer and the quantity of exchanged protons. Table 1 shows the results of ion-exchange experiment. The IEC of the composite Nafion/ZP membranes have an increased ion-exchange capacity (~40–50%) as compared to Nafion. Zirconium hydrogen phosphates have protons that can be exchanged which give the composite membrane a much greater ion-exchange capacity.

3.2. Water uptake and conductivity

Table 2 summarizes the water content of Nafion and Nafion/ZP composite membranes equilibrated with 100%

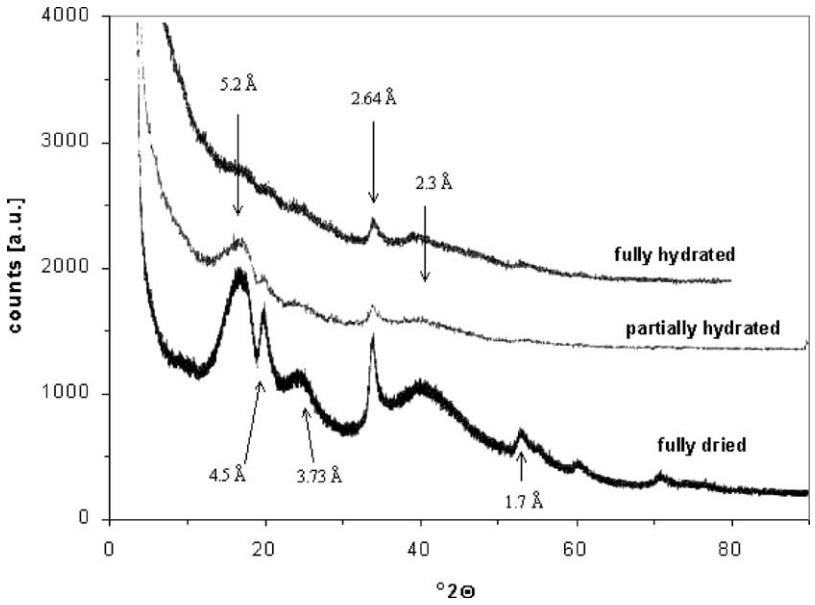

Fig. 2. X-ray diffraction patterns for Nafion 115/zirconium phosphate (25 wt.%) composite membranes. The broad peaks at 2.3 and 5.2 Å are attributed to crystalline stacking in the Teflon-rich microphases. The sharper features at 1.7, 2.64, and 4.5 Å are attributed to zirconium hydrogen phosphate.

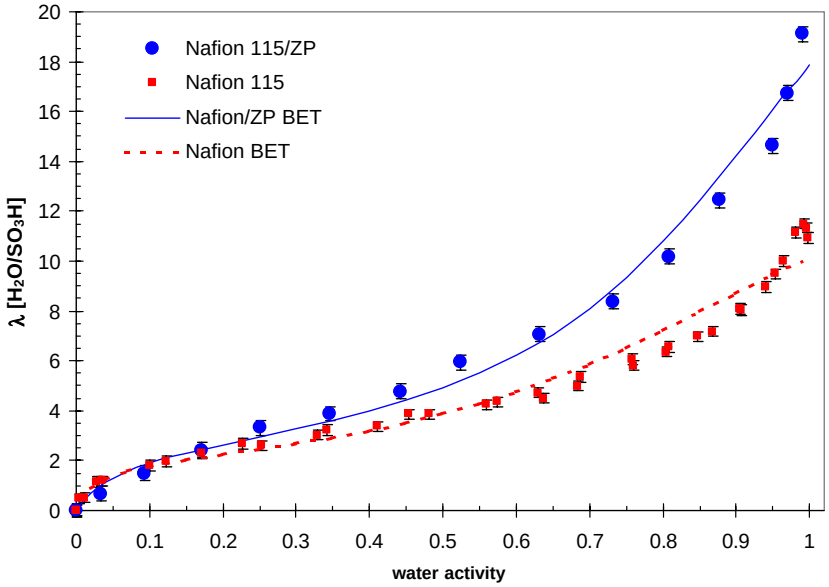

Fig. 3. Water uptake of Nafion 115 and Nafion 115/ZP (25 wt.%) composite membranes at 80 °C. The data were fit to finite layer BET isotherms (Eq. (7)) with fitting parameters—Nafion 115: $\lambda_m = 2$, $c = 35$, $n_L = 9.2$; Nafion/ZP composite: $\lambda_m = 2.6$, $c = 17$, $n_L = 12.8$.

relative humidity air at 80 °C and immersed in liquid water at 25 °C. Both these conditions correspond to water activity of 1. The membranes were removed from the water or the barometric sorption vessel and surface water is brushed off to get an accurate membrane water content measurement gravimetrically. The water content, λ, is calculated from the mass of water and Eqs. (4) and (5). Even though 100% relative humidity and liquid water both correspond to water activity of 1, there is a difference in the water uptake. Liquid water uptake is greater than water vapor uptake. This difference has been attributed to the osmotic pressure of the membrane swelling in the liquid that can increase water content considerably (Schroeder's paradox).

The water uptake isotherms at 80 °C for Nafion 115 and the Nafion/ZP composite membranes are shown in Fig. 3. As the water activity in the vessel is increased, the membrane water content increases. The isotherm shows a rapid rise at low water activity, a slow rising plateau at intermediate water activities, and the majority of water uptake occurring at high water activity $a_w > 0.6$. At 80 °C and water activity, $a_w = 1$, the Nafion membrane contains around 11 waters per sulfonate or about 18 wt.% of water. The solid line in Fig. 3 shows the results of the BET finite layer isotherm model describing the membrane water content dependence on relative humidity.

While the uptake of water from the extruded Nafion membranes has been characterized in the literature [7,43], water uptake by composite membranes has not received much attention. As seen in Fig. 3 the composite membrane contains more water than a Nafion membrane at the same water activity. The number of waters is based only on the sulfonic acid content in the Nafion and neglects the interaction of water with the zirconium phosphate. However, even on a total weight basis the Nafion/ZP membrane absorbs more water than Nafion.

The water uptake was not very sensitive to the temperature over the range 80–140 °C. Our data could not discern any change in the water uptake with temperature for fixed water activity.

The conductivity of Nafion 115 as a function or water activity over a range of temperatures from 80 to 140 °C is shown in Fig. 4. The data have been plotted on both log and linear scales. Most obvious from the log graph is the very large change in conductivity with water activity. The conductivity increases by five orders of magnitude with water activity increasing from 0 to 1. The conductivity values at $a_w = 0$ may be high because of incomplete water removal during the initial evacuation of the barometric sorption vessel can have a large impact. The most reliable conductivity measurements are for intermediate water activity, $0.15 < a_w < 0.95$, and the conductivity increases by more than two orders of magnitude with increasing water activity over that range. The temperature effect on conductivity is much smaller than the effect of water activity. By plotting the data on a linear scale the temperature effect becomes more evident. The conductivity increases by approximately a factor of 2 from 80 to 140 °C at fixed water activity.

We expected Nafion/zirconium phosphate membranes to have an increased conductivity compared to unmodified Nafion. The water content was higher in the composite membrane and the zirconium phosphate may contribute extra protons to increase the charge carrier concentration. Fig. 5 compares the conductivity of the Nafion/zirconium phosphate composite membrane with Nafion 115. The composite membranes had lower proton conductivity than Nafion over the entire range of water activities and temperatures. Similar to Nafion 115, the major conductivity change

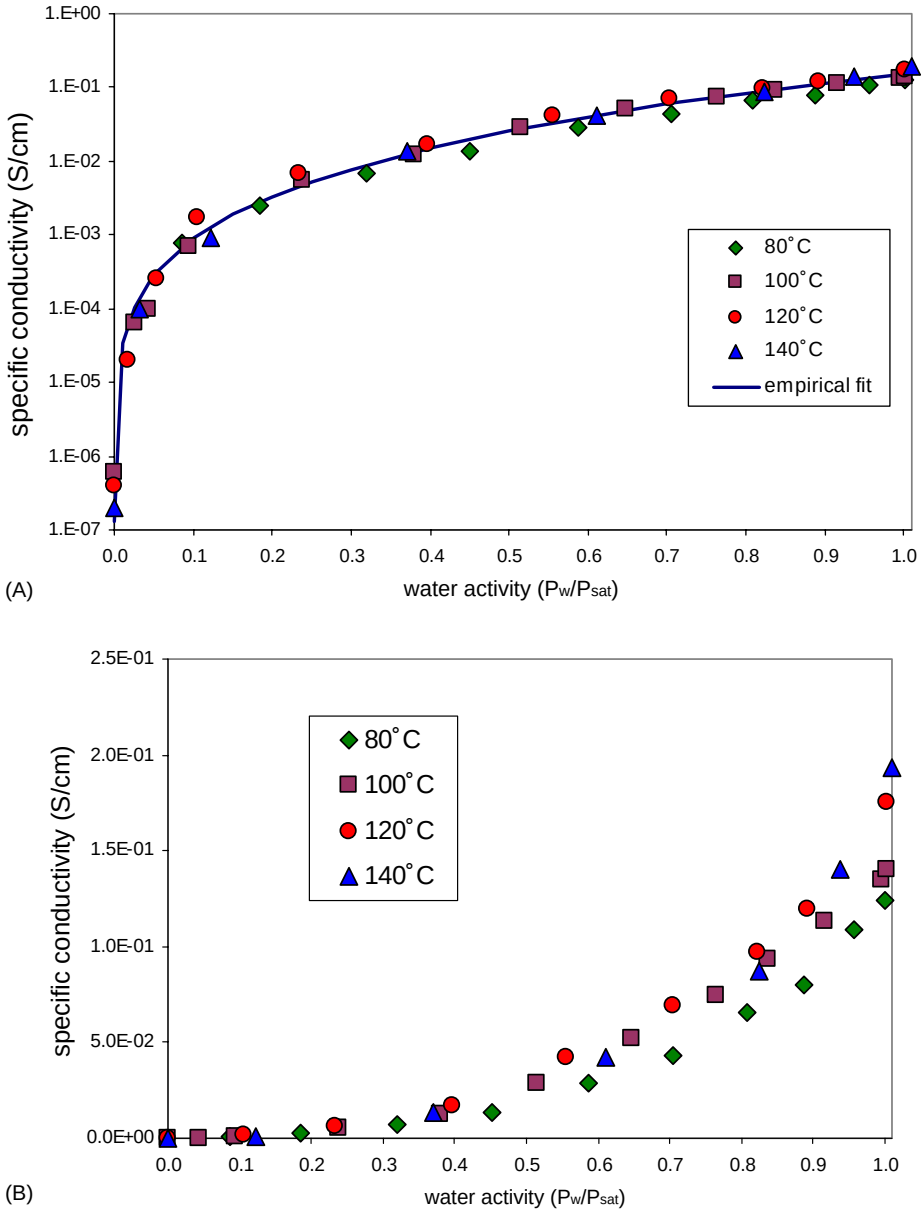

Fig. 4. (A) Conductivity of Nafion 115 as a function of water activity at temperatures from 80 to 140 °C. The empirical fit to the data is given by $\sigma = 1.3 \times 10^{-7} \exp(14a_w^{0.2})$ S/cm. (B) Conductivity of Nafion 115 as a function of water activity at temperatures from 80 to 140 °C. Data are replotted on a linear scale to accentuate the effect of temperature on the conductivity.

for the composite membrane is associated with the water activity. The conductivity of the composite membranes increased with temperature, but the variation of the composite membrane conductivity with temperature was slightly less than that observed with Nafion 115.

3.3. Small angle X-ray scattering

The slit collimated scattering data collected by the multi-channel detector were converted into the scattering intensity versus scattering angle. The raw data were analyzed to account for several factors following the procedure recommended by Register and Bell [40]:

(i) Scattering due to interaction with the helium sample environment was subtracted.
(ii) The absolute scattering intensity of the sample was determined quantitatively with a standard polyethylene sample.
(iii) The data were desmeared to correct for the slit width.

The invariant scattering intensity (q^2I) profile is plotted against Bragg spacing (determined from the scattering angle) for each membrane sample as a function of water content, λ, in Fig. 6. The data obtained show that increasing water content leads to an increase in the intensity of the scattering peaks for both an extruded Nafion 115 and a Nafion 115/ZP

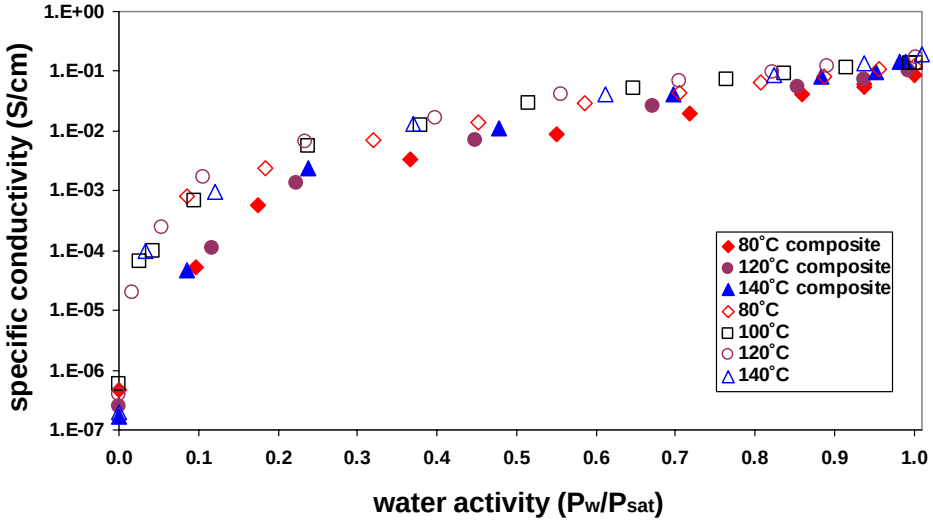

Fig. 5. Comparison of conductivity of Nafion/ZP composite membranes to Nafion 115. The conductivity at temperatures from 80 to 140 °C is plotted. The solid symbols are for the composite membrane and the open symbols are for Nafion 115.

composite membrane. The scattering intensity increases linearly with water content. Ionomers, such as Nafion, will micro-phase separate into a Teflon-like region and an ionic region containing the sulfonic acid groups [6,44–46]. In the pure Nafion membranes, the electron density of the ionic inclusions is slightly lower than that of the polymer backbone while in the zirconium phosphate composite membrane the electron densities of the two phases are almost equal. For this reason there is little electron density contrast between the two phases when the membranes are dry and no scattering peak is obtained [47]. Water has a significantly lower electron density than the fluorocarbon polymer matrix. Absorbed water partitions into the ionic regions of Nafion. As a result, the electron density contrast between the ionic and Teflon-like phases of Nafion increases with increasing water content, resulting in greater scattering intensity and an increasingly well-defined scattering peak [45].

The scattering peaks for the zirconium phosphate membrane in Fig. 6B are significantly wider than the peaks for the unmodified Nafion 115 membrane, indicating greater structural heterogeneity. In addition, the shift in the spacing between inclusions with water content is much less for the composite membrane than for Nafion. The maximum spacing between ionic inclusions at the highest water content is nearly the same for the Nafion 115 and the Nafion 115/ZP composite. The scattering maximum for Nafion shifts to smaller spacing with decreasing water content; however, the scattering maximum for the composite membrane is almost unchanged with decreasing water content.

3.4. Water transport

The flux of water through the membranes as a function of the nitrogen flow through the test cell is shown in Fig. 7. The Nafion 117 membrane has almost the same thickness as the Nafion 115/ZP composite membrane, permitting us to distinguish between the effects of membrane thickness and membrane composition. The data in Fig. 7 show that the water flux increases with nitrogen flow rate through the test cell at low flow rates and then plateaus at a limiting flux. The limiting flux corresponds to the minimum mass transfer resistance at the membrane gas interface, and diffusion through the membrane is the dominant mass transfer resistance. The limiting flux is greatest for the Nafion 115 membrane. The flux was reduced through the Nafion 117 membrane due to increased membrane thickness. The limiting water flux through the composite membrane is less than that for Nafion 117 suggesting that water diffusion through the composite membrane is reduced relative to diffusion through Nafion.

3.5. Fuel cell performance of Nafion/zirconium phosphate composite membranes

Polarization curves for fuel cells with membrane electrode assemblies containing Nafion 115 and Nafion 115/zirconium phosphate membranes were measured at four different sets of operating conditions. The base case was for humidified feeds near water activity of 1 with a cell temperature of 80 °C and pressure of 1 bar. The other three conditions were at elevated temperature and a total pressure of 3 bar. The conditions tested are defined by the total pressure in the fuel cell and the temperature of the humidifier bottle for the anode feed (T_{anode}), the cell temperature (T_{cell}), and the temperature of the humidifier bottle for the cathode ($T_{cathode}$).

Polarization curves are shown in Fig. 8 for fuel cells with Nafion 115 and Nafion 115/zirconium phosphate membranes at conditions 1 and 3. At 80 °C the fuel cell performance was nearly identical for both membranes, with the effective MEA resistance being slightly greater for the composite membrane than Nafion 115. When the temperature was

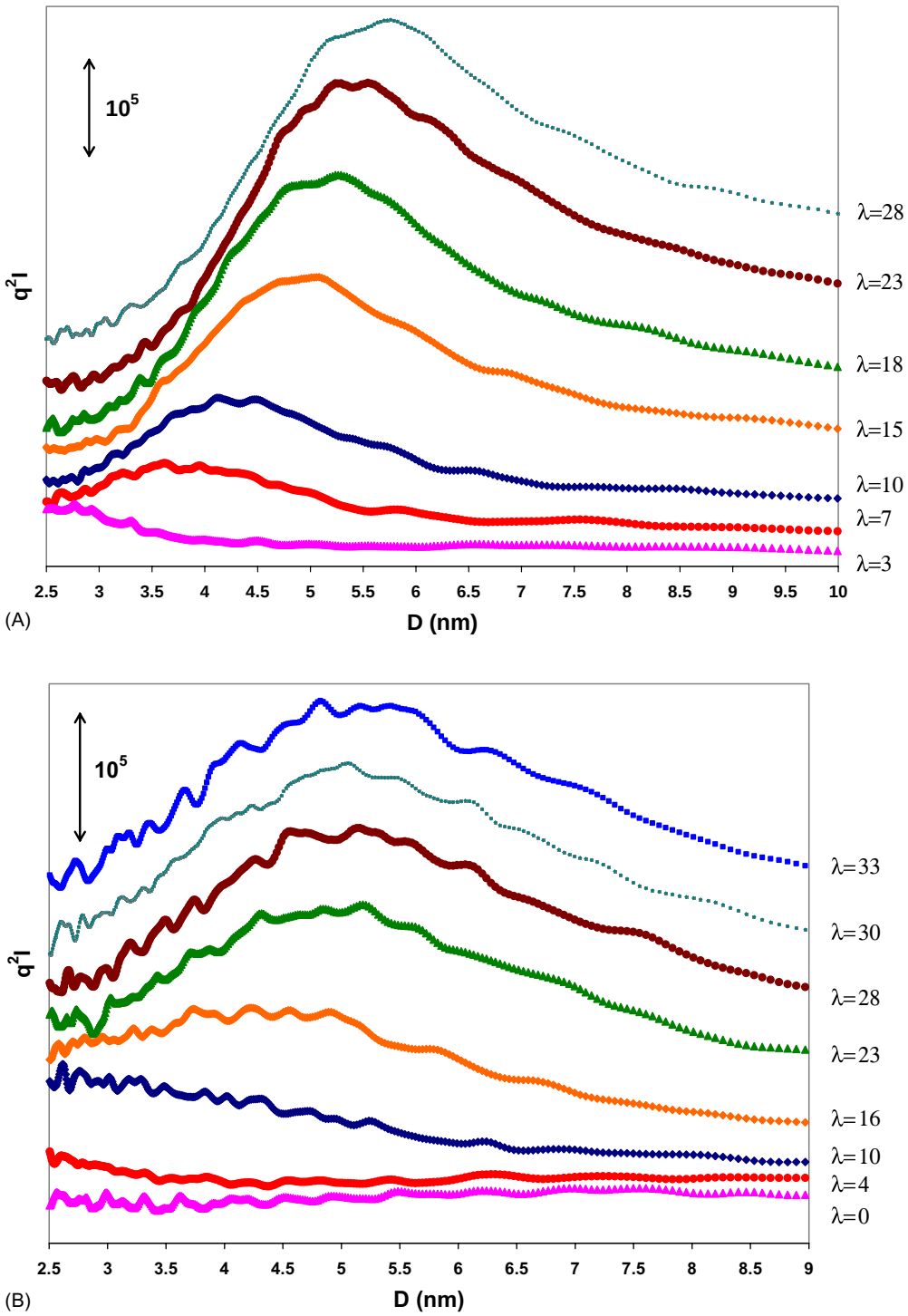

Fig. 6. (A) SAX scattering intensity (q^2I) for extruded Nafion 115 film. The scattering peaks result from water absorbed into the Nafion clustering creating electron density contrast with the fluorocarbon phase. The water content as determined by weight is given by the parameter λ. (B) Scattering intensity (q^2I) vs. Bragg spacing for the composite Nafion/zirconium phosphate (25 wt.%) membrane. The water content as determined by weight is given by the parameter λ.

130 °C the MEA resistance was substantially less for the composite membrane than for the Nafion 115 membrane.

The polarization curves for fuel cells with Nafion 115 and Nafion 115/zirconium phosphate composite membranes at different levels of humidification are shown in Fig. 9. By maintaining the humidification temperatures fixed the water vapor pressure of the feeds are fixed. At fixed feed humidification increasing the cell temperature will decrease the water activity in the cell, $a_w = P_w/P_{sat}(T_{cell})$. The effective MEA resistance increased less with decreased water activity

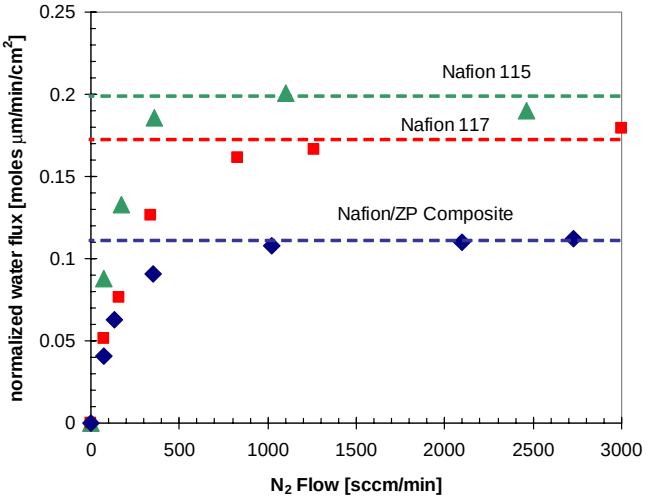

Fig. 7. Water flux through Nafion 115, Nafion 117, and Nafion 115/zirconium phosphate composite membranes as functions of gas flow on the opposite side of the membrane. The limiting fluxes are denoted by the horizontal lines.

for the composite membrane than observed with the Nafion 115 membrane.

The MEA polarization curves have been fitted to Eq. (5):

$$E = E_{\text{rev}} - b \log\left(\frac{i}{i_0}\right) - R_{\text{MEA}} i \tag{5}$$

where E_{rev} is the reversible cell potential, b the Tafel slope, i_0 the exchange current density, i the current density and R_{MEA} the membrane electrode resistance. The fit parameters at different operating conditions are summarized in Table 3. The composite membranes show reduced exchange current density compared to the Nafion membranes. The MEA resistance of the composite membranes is substantially less than the resistance of Nafion 115 at the higher fuel cell temperatures.

The composite membranes operated more stably at elevated temperatures. The cell was operated at 130 °C for 1 h, and then the cell temperature was raised to 140 °C. After 1 h of operation under the latter condition, the cell temperature was returned to 130 °C. After this procedure with the composite membrane the current–voltage curves returned to their initial (pre-140 °C operation) values. The unmodified Nafion 115 membranes, by contrast, were altered by the brief exposure (∼20–30 min) to the high temperature. The effective ohmic resistance of the Nafion 115 MEA increased from 1.3 to over 2 Ω after operation at 140 °C.

4. Discussion

When we initiated our studies with composite membranes the working hypothesis was that addition of zirconium phosphate to Nafion would increase the water uptake by the membrane at elevated temperature, thereby increasing the proton conductivity and thus improving the fuel cell performance. We were surprised that the proton conductivity was diminished in the composite membrane relative to Nafion in spite of the increased water uptake, and we were even more surprised that the fuel cell performance of the composite membranes exceeded Nafion even though the proton conductivity was reduced. Our data do not fully resolve these conflicting observations, but the data are consistent with the suggestion that mechanical properties of the composite membranes may be the key to the performance of composite membranes.

4.1. Water uptake and ion-exchange capacity

The ion-exchange capacity of the composite membrane is greater than the ion-exchange capacity of Nafion [48,49]. Zirconium phosphate has exchangeable protons; the number of protons depends on the chemical form of the zirconium phosphate. The ion-exchange capacity for the composite membrane listed in Table 1 can be divided into contributions

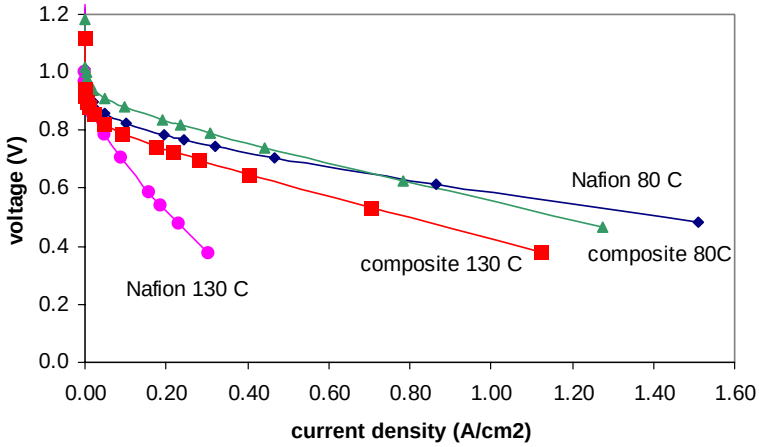

Fig. 8. Comparison of PEM fuel cell performance with MEA containing Nafion 115 and Nafion 115/zirconium phosphate composite membranes. The operating conditions are listed in Table 3. Operating condition 1 at 80 °C and operating condition 3 at 130 °C.

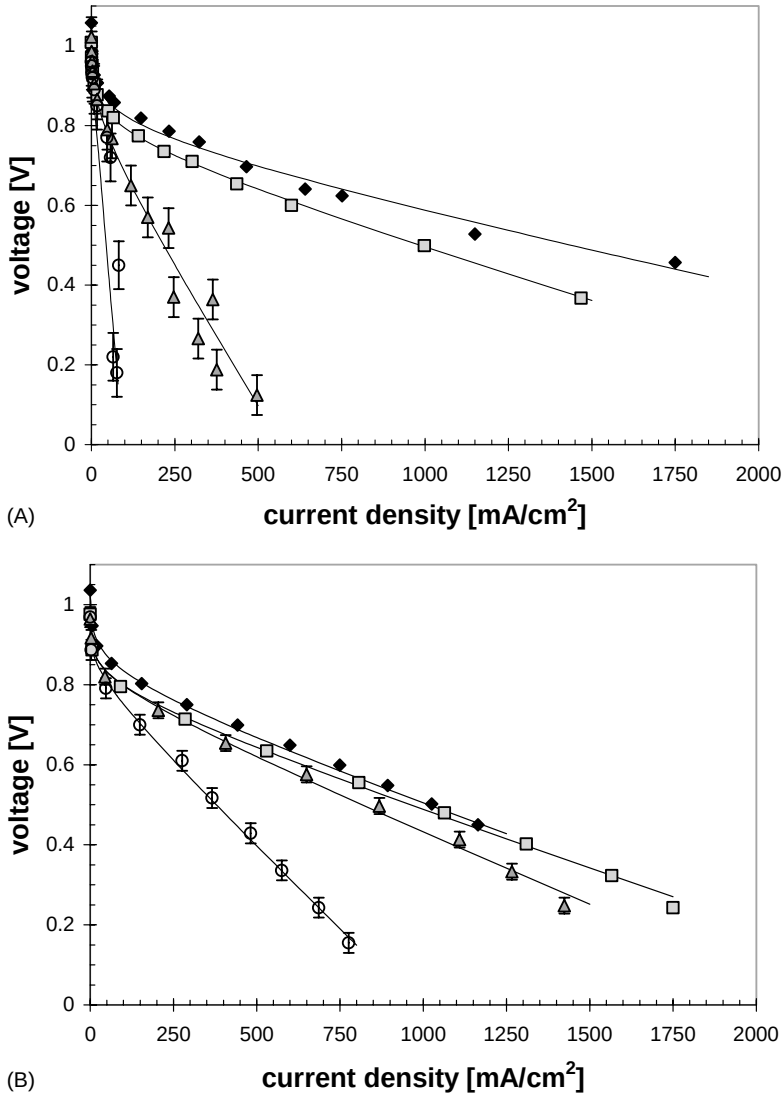

Fig. 9. (A) PEM fuel cell performance of an MEA employing a Nafion 115 membrane. The cell voltage is plotted as a function of average current density in the fuel cell. The cell operating conditions are: (◆) 1; (□) 2; (▲) 3; (○) 4. (B) PEM fuel cell performance of an MEA employing a Nafion 115/ZP composite membrane. The cell voltage is plotted as a function of average current density in the fuel cell. The cell operating conditions are: (◆) 1; (□) 2; (▲) 3; (○) 4.

Table 3
Fuel cell performance parameters

Membrane	Operating condition	b (mV/dec)	$i_0 \cdot (\times 10^3$ mA/cm^2)	R_{MEA} (Ω cm^2)
Nafion 115	1	84.7	3.7	0.17
	2	82.0	4.6	0.24
	3	93.4	13.7	1.3
	4	–	–	9.8
Nafion 115/zirconium phosphate (25%)	1	55.0	3.0	0.3
	2	66.4	0.6	0.27
	3	59.6	0.18	0.34
	4	55.1	0.06	0.79

Operating conditions: (1) $P = 1$ bar, $T_{anode}/T_{cell}/T_{cathode} = 90/80/88$; (2) $P = 3$ bar, $T_{anode}/T_{cell}/T_{cathode} = 130/120/130$; (3) $P = 3$ bar, $T_{anode}/T_{cell}/T_{cathode} = 130/130/130$; (4) $P = 3$ bar, $T_{anode}/T_{cell}/T_{cathode} = 130/140/130$.

from the Nafion and from the zirconium phosphate:

$$\mathrm{IEC_{composite}} = (\text{mass fraction Nafion})\mathrm{IEC_{Nafion}} + (\text{mass fraction ZrP})\mathrm{IEC_{ZrP}} \quad (6)$$

Assuming that the IEC of Nafion in the composite is unchanged the IEC for the zirconium phosphate in the membrane is 2670 μeq/g. $Zr(HPO_4)_2{\cdot}H_2O$ has an ion-exchange capacities of 6640 μeq/g. The ion-exchange capacity of the zirconium phosphate in the composite membrane is less than ZHP, suggesting that a mixture of different zirconium phosphate phases, including amorphous ZP, are formed in the composite membrane. XRD identified diffraction peaks that correspond to crystalline zirconium hydrogen phosphate, but most of the zirconium phosphate was amorphous and XRD cannot quantify the amorphous zirconium phosphate.

Liquid water uptake by Nafion 115 and the Nafion115/ZP composite were the same when normalized by the sulfonic acid concentration. The mass uptake of liquid water normalized by the mass fraction of Nafion in the membrane is the same in both membranes.

Water uptake from the vapor is reduced compared to water uptake from liquid water. The composite membranes showed substantially greater water uptake from the vapor phase than water uptake by Nafion 115. The water uptake as a function of water activity, shown in Fig. 3, was fit by a finite layer BET isotherm [27]:

$$\lambda = \lambda_m \frac{[ca_w][1-(n_L+1)(a_w^{n_l}+n_l a_w^{n_L+1})]}{(1-a_w)[1+(c-1)a_w - ca_w^{n_l+1}]} \quad (7)$$

λ_m is the monolayer coverage of water on the sulfonic acid groups, c is related to the chemical potential change due to water adsorption, and n_L the number of layers that can be adsorbed. The parameters to fit the water uptake isotherms are shown in Fig. 3. The data fits suggest that the more water can be adsorbed in the composite compared to Nafion, both in the monolayer (first salvation shell—larger λ_m) and in the multilayer (larger n_L); however, the reduction of c for the composite membrane relative to Nafion suggests that the water is less strongly adsorbed in the composite membrane.

Why should the composite membrane absorb more water from the vapor phase than Nafion? SAXS data in Fig. 6 show that the distance between the ionic inclusions in the composite membrane changed less than Nafion 115 with increased water content. The scattering peak shifts from 4.5 to 5.1 nm in the composite membrane, and from 3.7 to 5.1 nm in Nafion 115. The zirconium phosphate is formed when the membrane is fully hydrated, and the distance between the hydrophilic inclusions is at ~5.1 nm. When the membrane is dried, the Nafion contracts but the zirconium phosphate does not. The zirconium phosphate appears to act as scaffold so the membrane cannot shrink much when the water is removed. During rehydration the composite membrane does not swell much because the inorganic scaffold has kept it extended.

The scaffolding effect of the membrane also explains why the water vapor uptake by the composite membrane is greater. When the Nafion 115 membrane absorbs water it must do work to swell the membrane, the composite membrane is already in a partially swelled state, so less work has to be done to swell the membrane, resulting in greater water uptake. The scaffolding effect also explains the reduced density of the dry composite membrane relative to both Nafion and zirconium phosphate. The scaffolding maintains the dimension of the membrane from the swollen state, so as the water is removed void volume is created. The void volume reduces the bulk density of the membrane.

4.2. Proton conductivity

Protons are transported through the membrane by two pathways. The first is a proton shuttling (or Grotthus) mechanism that involves the formation and breaking of hydrogen bonds between the proton and water [50,51]. The second pathway for proton conduction is equivalent to traditional cation conduction where the hydrated proton diffuses through the aqueous media in response to an electrochemical gradient [52,53]. The proton conductivity via the Grotthus mechanism is considerably faster than hydronium ion diffusion, and it is estimated that approximately 90% of proton conductance occurs via the Grotthus pathway [50].

We fit our proton conductivity data to two models from the literature in an effort to identify the role of the zirconium phosphate in proton conductivity. The random network model for membrane proton conductivity proposed by Eikerling et al. [26] is based upon the inverted micelle structure of Nafion and other ionomer membranes. The micelles, or "pores", are either dry with low conductivity or wet with high conductivity. As a membrane absorbs water and swells, the fraction of wet pores in the membrane increases, while the fraction of dry pores decreases. The distributions of wet and dry pores are governed by the membrane water content and swelling behavior.

The Eikerling model uses a single-bond effective medium approximation (SB-EMA) to solve for the conductivity of this random network. Swelling and structural changes (i.e. ionic cluster reorganization) within the membrane are described by Eqs. (8) and (9):

$$n(w) = n_0(1+\alpha w) \quad (8)$$

$$\upsilon(w) = \upsilon_0(1+\beta w)^3 \quad (9)$$

$n(w)$ is the number of sulfonic acid groups in an average pore, n_0 the number of sulfonic acid groups in the average pore of a dry membrane, $\upsilon(w)$ the average volume of the pore, υ_0 the pore volume in the dry membrane, w the water content of the membrane in weight percent, and the parameters α and β are used to describe the extent of the swelling and reorganization in the membrane. The fraction of wet

Table 4
Proton conductivity model of Eikerling

Membrane	Fitting parameters				
	α	β	γ	$\sigma_{wet}/\sigma_{dry}$	$\sigma_{x=1} = \sigma_{wet}$
Nafion 115	0.0693	0.034	0.10	930	0.14
Nafion/zirconium phosphate	0.0198	0.017	0.07	600	0.12

pores, $x(w)$, depends on the water fraction, the swelling parameters and a scaling parameter, γ:

$$x(w) = \frac{\gamma w}{(1+\beta w)^3 - \gamma w^2 \alpha} \quad (10)$$

The conductivity of the membrane is the weighted average of the conductivities of the wet and dry pores:

$$\sigma = x(w)\sigma_{wet} + (1 - x(w))\sigma_{dry} \quad (11)$$

The small angle X-ray scattering data and the cluster swelling model proposed by Gierke and Hsu [54] were employed to calculate the values for the number of sulfonates per pore and the pore volume (n and υ) as a function of water content, w. The calculated values of n and υ were plotted as a function of w and the best fit for parameters α and β were calculated. The parameter γ was obtained by equating $x(w) = 1$ when $w = 0.41$ in Eq. (10). Table 4 shows the parameter values obtained from the SAXS data and conductivity at saturation. A critical caveat in determining these swelling parameters is that the SAXS data were collected at room temperature (25 °C), while it is being applied to the membrane conductivity model at 80 °C.

The model fit to the experimental conductivity data is shown in Fig. 10. The model consistently overestimates the conductivity. The values of the swelling parameters α and β are less for the composite membrane than those obtained for Nafion 115, which reflect the decreased swelling of the composite membrane. The conductivity of the dry pores is nearly an order of magnitude greater for the composite membrane than for Nafion 115.

Thampan et al. presented an alternative model for proton conductivity in ionomers [27]. This model is analogous to proton diffusion in an aqueous electrolyte; it introduces a correction factor to account for the presence of the polymer matrix. The basic assumptions are:

(i) The additional frictional interaction with the polymer membrane is modeled as proton diffusion through both water and large polymer particles.
(ii) The introduction of a percolation threshold below which no conduction can take place because of the lack of a continuous conduction pathway.
(iii) Effective diffusion constants are introduced to account for the porosity and tortuosity of the polymer matrix.

Table 5
Proton conductivity model of Thampan et al.

Parameter	Value for Nafion 115	Value for Nafion/ZP composite
ε_0	0.025	0.045
q	1.5	1.5
$c_{HA,0}$ ($\times 10^{-3}$ cm^{-3})	1.98	2.93
$K_{dissociation}$	6.2	6.2
λ_1^0 (at 353 K)	1650	1650
δ	0.4	3.7

The model yields the following equations that describe the conductivity of a proton conducting membrane:

$$\sigma = (\varepsilon - \varepsilon_0)^q \left(\frac{\lambda_1^0}{1+\delta}\right) c_{HA,0}\alpha \quad (12)$$

where ε is the fractional membrane volume filled with water and ε_0 the fractional membrane volume corresponding to the percolation threshold, q is a fitted constant, $c_{HA,0}$ the concentration of sulfonic acid groups, δ the ratio of diffusion coefficients (D_{H^+,H_2O} and $D_{H^+,membrane}$), λ_1^0 the equivalent conductance at infinite dilution in water, and α the fractional dissociation of the sulfonic acid in the membrane, which is a function of water content.

The theoretical relationship between water content and membrane proton diffusion coefficients has not been adequately delineated in the literature, although some empirical fits have been proposed [55]. Thampan used δ as a fitting parameter to improve the model fit to literature conductivity data.

In our analysis we used the values suggested by Thampan et al. listed in Table 5. The only parameter that we modified between the various membranes is δ. Fig. 10A and B shows the model results compared with experimental conductivity versus water content data.

The model does a fair job at reproducing the experimental data. As the membrane water content increases the sulfonic acid residues dissociate increasing the concentration of protons in the membrane and increasing the conductivity. The predicted conductivity decreases faster with decreased water content than the experimental data. The composite membranes has a larger δ values compared to unmodified Nafion. The determination of the best fit δ values suggests that there is a factor of 2–3 decrease in the diffusion coefficient for protons through the "polymer" portion of the composite membrane at given water content. This decrease is much more than the decrease in the water diffusion suggested by the water transport experiments.

The water transport through the composite membrane is 35% less than water transport through the Nafion 117 membrane. Those two membranes have comparable thickness. If water diffusion is limited to the organic phase of the composite, then the water transport data suggest that the zirconium phosphate plays no role in water diffusion.

The Thampan model as well as the models of Gierke et al. [45] and Paddison [56] assume a threshold water content

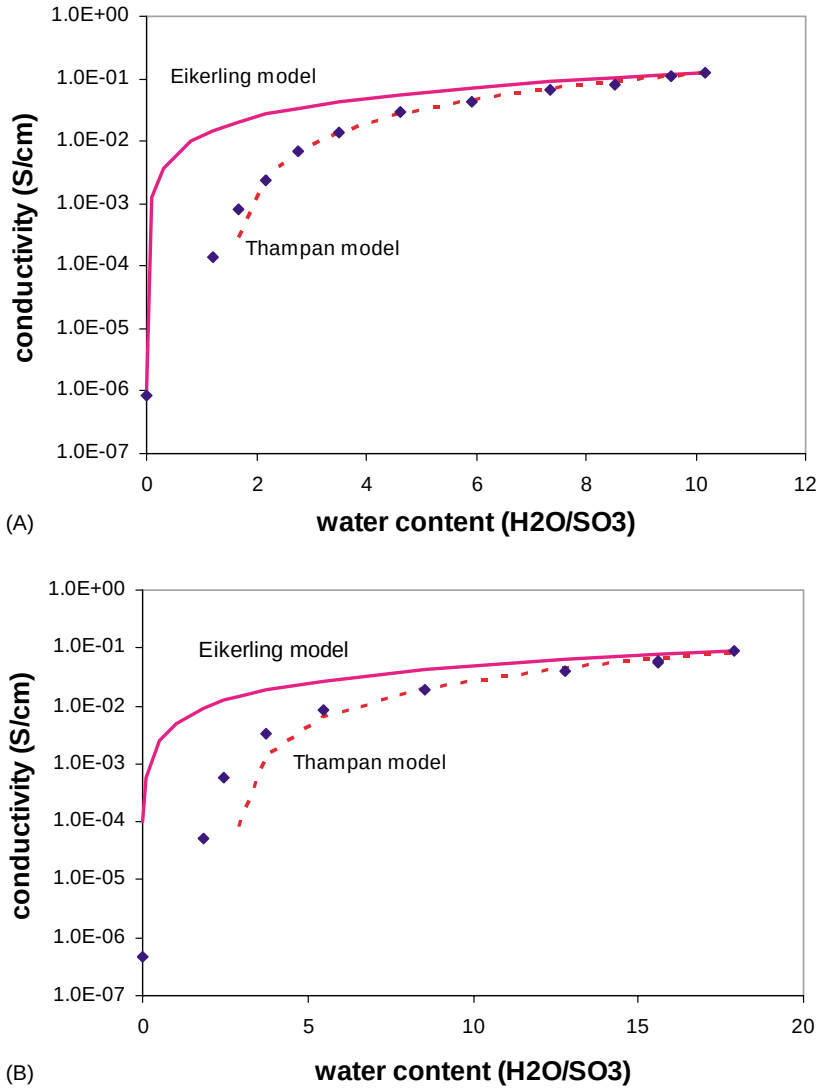

Fig. 10. (A) Model fits of the proton conductivity in Nafion 115. The solid line is the fit by the model of Eikerling et al. (Eqs. (7)–(10)) with the parameters given in Table 4. The dotted line is the model of Thampan et al. (Eq. (11)) with the parameters given in Table 5. The points are the experimental data. (B) Model fits of the proton conductivity in Nafion 115/zirconium phosphate composite membrane. The solid line is the fit by the model of Eikerling et al. (Eqs. (7)–(10)) with the parameters given in Table 4. The dotted line is the model of Thampan et al. (Eq. (11)) with the parameters given in Table 5. The points are the experimental data.

below which no proton conduction occurs. Experimentally Nafion membranes have a small but non-zero conductivity even at "zero" water content. The model presented by Thampan et al. neglects tunneling and other diffusion mechanisms that may dominate at low water content. We have shown a single parameter empirical fit to the conductivity data for Nafion in Fig. 4A:

$$\sigma = \sigma_{a_w=0} \exp(c_1 a_w^{c_2}) \quad (13)$$

$\sigma_{a_w} = 0$ is the conductivity of a dry membrane, $c_1 = \ln(\sigma_{a_w=1}/\sigma_{a_w=0})$, and c_2 is an adjustable parameter. This empirical equation fits the conductivity as a function of water activity very well with only one adjustable parameter. The empirical fit is useful for modeling PEM fuel cells.

4.3. Fuel cell performance

The most surprising result from our studies is that fuel cell performance, as judged by the polarization curves, is improved for composite membranes even though the proton conductivity is poorer. This improvement in fuel cell performance appears to be limited to conditions where the water activity is significantly less than 1. We estimated the water activity in the fuel cell for different temperatures of the humidifier bottles assuming the same mass transfer efficiency at the different temperatures. (The mass transfer efficiency was estimated from a separate experiment where dry air flowing at 100 mL/min was bubbled through the humidifier at 50 °C and the outlet humidity was measured.) The

estimated water vapor pressure of the gases humidified at 140, 130, and 120 °C are 2.4, 2.0, and 1.7 bar, respectively, so the water activity in the fuel cell for the three cases are $a_w(140/130/140) = 1.0$, $a_w(130/130/130) = 0.85$, and $a_w(120/130/120) = 0.70$.

Reducing the water activity from 1.0 to 0.7 should increase the membrane resistance for Nafion 115 from 0.20 to 0.22 $\Omega\,cm^2$. However, from the fuel cell data the membrane resistance increased from 0.24 to 9.8 $\Omega\,cm^2$. The increase in the effective MEA resistance is much greater than that predicted from the conductivity measurements. Why is there such a large discrepancy and why does the effective MEA resistance only increase from 0.27 to 0.79 $\Omega\,cm^2$ for the composite membrane?

We suggest that the discrepancy is due to the constrained environment of the membrane in the fuel cell. The MEA is compressed between the bipolar plates. The applied pressure on the MEA limits the swelling of the membrane. Absorbed water swells the membrane creating a "swelling pressure" that must overcome the applied sealing pressure of the fuel cell. The greater the water activity the greater the swelling pressure exerted by the membrane. In the fuel cell environment the water content of the membrane is probably much less than that expected based on ex situ measurements because the sealing pressure squeezes water from the membrane.

We suggested that the zirconium phosphate in the composite membrane forms rigid internal scaffolding, which would resist compression of the sealing pressure. At the reduced water activity the composite membrane can take up water and swell without having to overcome the applied sealing pressure. We suggest that the zirconium phosphate provides mechanical strength to the membrane; the data suggest that the zirconium phosphate plays little role in the actual conduction of protons through the membrane. This explanation is also consistent with our group's results with other Nafion/metal oxide composite membranes. We have routinely found improved fuel cell performance of the composite membranes at reduced water activity, and there has been little sensitivity to the choice of metal oxide [57–59].

The effect of clamping the fuel cell is accentuated at higher temperatures because the elastic modulus of the membrane decreases with increasing temperature. The glass transition temperature of dry Nafion is ~100–110 °C, and decreasing with water content. Above the glass transition temperature the swelling pressure is greatly reduced.

5. Conclusions

Nafion 115/zirconium phosphate composite membranes show enhanced fuel cell performance compared to Nafion 115 at elevated temperature and reduced water activity. A Nafion 115/zirconium phosphate composite membrane had a greater ion-exchange capacity and took up more water than Nafion 115 membranes, but the composite membranes showed reduced proton conductivity and water transport. Small angle X-ray scattering data indicated that the spacing between hydrophilic phases in the composite membrane were further apart than in Nafion 115, and there appeared to be less restructuring of the composite membrane with water absorption. The data suggest that the zirconium phosphate forms an internal rigid scaffold within the membrane that permits increased water uptake by the membrane in the confined environment of the fuel cell membrane electrode assembly.

Acknowledgements

We thank Professor Richard Register for his assistance with the SAXS measurements. We also acknowledge financial support from NSF DMR-0213707 through the Materials Research Science and Engineering Center at Princeton.

References

[1] EG&G Services P., Inc., Fuel Cell Handbook, Contract No. DE-AM26-99FT40575, US Department of Energy, Morgantown, WV, October 2000, 312 pp.
[2] L.J.M.J. Blomen, M.N. Mugerwa (Eds.), Fuel Cell Systems, Plenum Press, New York, 1993, 614 pp.
[3] S. Srinivasan, B.B. Dave, K.A. Murugesamoorthi, A. Parthasarathy, A.J. Appleby, Overview of fuel cell technology, in: L.J.M.J. Blomen, M.N. Mugerwa (Eds.), Fuel Cell Systems, Plenum Press, New York, 1993, pp. 37–72.
[4] S. Mukerjee, S. Srinivasan, Enhanced electrocatalysis of oxygen reduction on platinum alloys in proton exchange membrane fuel cells, J. Electroanal. Chem. 357 (1993) 201–224.
[5] Q.F. Li, R.H. He, J.O. Jensen, N.J. Bjerrum, Approaches and recent development of polymer electrolyte membranes for fuel cells operating above 100 °C, Chem. Mater. 15 (26) (2003) 4896–4915.
[6] S.C. Yeo, A. Eisenberg, Physical properties and supermolecular structure of perfluorinated ion-containing (Nafion) polymers, J. Appl. Polym. Sci. 21 (4) (1977) 875–898.
[7] J.T. Hinatsu, M. Mizuhata, H. Takenaka, Water uptake of perfluorosulfonic acid membranes from liquid water and water vapor, J. Electrochem. Soc. 141 (6) (1994) 1493–1498.
[8] L.A. Zook, J. Leddy, Density and solubility of Nafion: recast, annealed, and commercial films, Anal. Chem. 68 (21) (1996) 3793–3796.
[9] C. Yang, P. Costamagna, S. Srinivasan, J. Benziger, A.B. Bocarsly, Approaches and technical challenges to high temperature operation of proton exchange membrane fuel cells, J. Power Sources 103 (1) (2001) 1–9.
[10] G. Alberti, M. Casciola, Composite membranes for medium-temperature PEM fuel cells, Annu. Rev. Mater. Res. 33 (2003) 129–154.
[11] K.T. Adjemian, S.J. Lee, S. Srinivasan, J. Benziger, A.B. Bocarsly, Silicon oxide Nafion composite membranes for proton-exchange membrane fuel cell operation at 80–140 °C, J. Electrochem. Soc. 149 (3) (2002) A256–A261.
[12] P.L. Antonucci, A.S. Arico, P. Creti, E. Ramunni, V. Antonucci, Investigation of a direct methanol fuel cell based on a composite Nafion-silica electrolyte for high temperature operation, Solid State Ionics 125 (1999) 431–437.
[13] M. Doyle, S. Choi, G. Proulx, High-temperature proton conducting membranes based on perfluorinated ionomer membrane–ionic liquid composites, J. Electrochem. Soc. 147 (1) (2000) 34–37.

[14] W.G. Grot, G. Rajendran, Membranes containing inorganic fillers and membrane and electrode assemblies and electrochemical cells employing same, US Patent 5 919 583 (6 July 1999).
[15] I. Honma, S. Hirakawa, K. Yamada, J.M. Bae, Synthesis of organic/inorganic nanocomposites protonic conduction membranes through sol–gel processing, Solid State Ionics 118 (1999) 29–36.
[16] S.J. Lee, K.T. Adjemian, A.B. Bocarsly, S. Srinivasan, in: Novel Membranes for PEMFC Operation above 100 °C, The Elecrochemical Society Meeting, Toronto, Canada, 14–18 May 2000, The Electrochemical Society, Toronto, Canada, 2000.
[17] S. Malhotra, R. Datta, Membrane-supported nonvolatile acidic electrolytes allow higher temperature operation of proton-exchange membrane fuel cells, J. Electrochem. Soc. 144 (2) (1997) L23–L26.
[18] K.A. Mauritz, Organic–inorganic hybrid materials: perfluorinated ionomers as sol–gel polymerization templates for inorganic alkoxides, Mater. Sci. Eng. 6 (1998) 121–133.
[19] N. Miyake, J.S. Wainright, R.F. Savinell, Evaluation of a sol–gel derived Nafion/silica hybrid membrane for proton electrolyte membrane fuel cell applications. I. Proton conduction and water content, J. Electrochem. Soc. 148 (8) (2001) 898–904.
[20] O.J. Murphy, A.J. Cisar, Composite membrane suitable for use in electrochemical devices, US Patent 6 059 943 (9 May 2000).
[21] Y. Si, J.-C. Lin, H.R. Kunz, J.M. Fenton, in: $Zr(HPO_4)_2$—Nafion Composite Membranes for Direct Methanol Fuel Cells, Meeting of the Electrochemical Society, Philadelphia, PA, 12–17 May 2002, Electrochemical Society, Philadelphia, PA, 2002.
[22] K.A. Mauritz, J.T. Payne, [Perfluorosulfonate ionomer]/silicate hybrid membranes via base-catalyzed in situ sol–gel processes for tetraethylorthosilicate, J. Membrane Sci. 168 (1–2) (2000) 39–51.
[23] I. Honma, O. Nishikawa, T. Sugimoto, S. Nomura, H. Nakajima, A sol–gel derived organic/inorganic hybrid membrane for intermediate temperature PEFC, Fuel Cells 2 (1) (2002) 52–58.
[24] W.G. Grot, G. Rajendran, Membranes containing inorganic fillers and membrane electrode assemblies and electrochemical cells employing same, US Patent 5 919 503 (6 July 1999).
[25] G. Alberti, M. Casciola, R. Palombari, Inorgano–organic proton conducting membranes for fuel cells and sensors at medium temperatures, J. Membrane Sci. 172 (1–2) (2000) 233–239.
[26] M. Eikerling, Y.I. Kharkats, A.A. Kornyshev, Y.M. Volfkovich, Phenomenological theory of electro-osmotic effect and water management in polymer electrolyte proton-conducting membranes, J. Electrochem. Soc. 145 (8) (1998) 2684–2699.
[27] T. Thampan, S. Malhotra, H. Tang, R. Datta, Modeling of conductive transport in proton-exchange membranes for fuel cells, J. Electrochem. Soc. 147 (9) (2000) 3242–3250.
[28] G. Alberti, M. Casciola, S. Cavalaglio, R. Vivani, Proton conductivity of mesoporous zirconium phosphate, Solid State Ionics 125 (1999) 91–97.
[29] G. Alberti, L. Boccali, M. Casciola, L. Massinelli, E. Montoneri, Protonic conductivity of layered zirconium phosphonates containing $–SO_3H$ groups. III. Preparation and characterization of α-zirconium sulfoaryl phosphonates, Solid State Ionics 84 (1–2) (1996) 97–104.
[30] G. Alberti, M. Casciola, Layered $metal^{IV}$ phosphonates, a large class of inorgano–organic proton conductors, Solid State Ionics 97 (1–4) (1997) 177–186.
[31] G. Alberti, M. Casciola, U. Costantino, M. Leonardi, AC conductivity of anhydrous pellicular zirconium phosphate in hydrogen form, Solid State Ionics 14 (1984) 289–295.
[32] G. Alberti, M. Casciola, M.U. Costantino, A. Peraio, E. Montoneri, Protonic conductivity of layered zirconium phosphonates containing $–SO_3H$ groups. I. Preparation and characterization of a mixed zirconium phosphonate of composition $Zr(O_3PR)_{0.73}(O_3PR\ prime)_{1.27-nH2}$, with $R = –C_6H_4–SO_3H$ and R prime $= –CH_2–CH$, Solid State Ionics 50 (3–4) (1992) 315–322.
[33] G. Alberti, Syntheses, crystalline structure and ion-exchange properties of insoluble acid salts of tetravalent metals and their salt forms, Acc. Chem. Res. 11 (1978) 163–170.
[34] G. Alberti, M. Casciola, R. Palombari, A. Peraio, Protonic conductivity of layered zirconium phosphonates containing $–SO_3H$ groups. II. AC conductivity of zirconium alkyl-sulphophenyl phosphonates in the range 100–200 °C, in the presence or absence of water vapour, Solid State Ionics 58 (3–4) (1992) 339–344.
[35] X. Glipa, J.-M. Lelout, D.J. Jones, J. Roziere, Enhancement of the protonic conductivity of α-zirconium phosphate by composite formation with alumina or silica, Solid State Ionics 97 (1997) 227–232.
[36] M. Casciola, U. Costantino, Relative humidity influence on proton conduction of hydrated pellicular zirconium phosphate in hydrogen form, Solid State Ionics 20 (1986) 69–73.
[37] M. Casciola, F. Marmottini, A. Peraio, AC conductivity of a layered zirconium phosphate in the presence of water vapour at 100–200 °C, Solid State Ionics 61 (1–3) (1993) 125–129.
[38] T.-Y. Chen, J. Leddy, Ion exchange capacity of Nafion and Nafion composites, Langmuir 16 (2000) 2866–2871.
[39] A. Clearfield, J.A. Stynes, The preparation of crystalline zirconium phosphate and some observations on its ion exchange behaviour, J. Inorg. Nucl. Chem. 26 (1964) 117–129.
[40] R.A. Register, T.R. Bell, Miscible blends of zinc-neutralized sulfonated polystyrene and poly(2,6-dimethyl-1,4-phenylene oxide), J. Polym. Sci.: Polym. Phys. 30 (6) (1992) 569–575.
[41] A.S. Arico, P. Creti, P.L. Antonucci, V. Antonucci, Comparison of ethanol and methanol oxidation in a liquid-feed solid polymer electrolyte fuel cell at high temperature, Electrochem. Solid State Lett. 1 (2) (1998) 66–68.
[42] G. Alberti, U. Costantino, R. Millini, G. Perego, A.R. Vivani, Preparation, characterization and structure of α-zirconium hydrogen phosphate hemihydrate, J. Solid State Chem. 1 (113) (1994) 289–295.
[43] P. Futerko, I.M. Hsing, Thermodynamics of water uptake in perfluorosulfonic acid membranes, J. Electrochem. Soc. 146 (6) (1999) 2049–2053.
[44] W.Y. Hsu, T.D. Gierke, Ion clustering and transport in Nafion perfluorinated membranes, J. Electrochem. Soc. 129 (3) (1982) C121–C121.
[45] T.D. Gierke, G.E. Munn, F.C. Wilson, Morphology of perfluorosulfonated membrane products—wide-angle and small-angle X-ray studies, ACS Symp. Ser. 180 (1982) 195–216.
[46] K.D. Kreuer, On the development of proton conducting polymer membranes for hydrogen and methanol fuel cells, J. Membrane Sci. 185 (1) (2001) 29–39.
[47] E.J. Roche, M. Pineri, R. Duplexxis, A.M. Levelut, Small-angle scattering studies of Nafion membranes, J. Polym. Sci. 19 (1981) 1–11.
[48] G. Alberti, M. Casciola, S. Cavalaglio, R. Vivani, Proton conductivity of mesoporous zirconium phosphate pyrophosphate, Solid State Ionics 125 (1–4) (1999) 91–97.
[49] G. Alberti, M. Casciola, F. Marmottini, R. Vivani, Preparation of mesoporous zirconium phosphate-pyrophosphate with a large amount of thermally stable acid groups on the pore surface, J. Porous Mater. 6 (4) (1999) 299–305.
[50] J.O.M. Bockris, A.K. Reddy, Modern Electrochemistry, vol. 1, 2nd ed., Plenum Press, New York, 1998.
[51] D. Marx, M.E. Tuckerman, J. Hutter, M. Parrinello, The nature of the hydrated excess proton in water, Nature 397 (1999) 601–604.
[52] T.A. Zawodzinski, J. Davey, J. Valerio, S. Gottesfeld, The water content dependence of electro-osmotic drag in proton-conducting polymer electrolytes, Electrochim. Acta 40 (3) (1995) 297–302.
[53] M. Eikerling, A.A. Kornyshev, U. Stimming, Electrophysical properties of polymer electrolyte membranes: a random network model, J. Phys. Chem. B 101 (1997) 10807.
[54] T.D. Gierke, W.Y. Hsu, The cluster-network model of ion clustering in perfluorosulfonated membranes, in: A. Eisenberg, H.L. Yeager (Eds.), Perfluorinated Ionomer Membranes, ACS, Washington, DC, 1982, pp. 283–307.

[55] J.H.G. van der Stegen, A.J. van der Veen, H. Weerdenburg, J.A. Hogendoorn, Application of the Maxwell-Stefan theory to the transport in ion-selective membranes used in the chloralkali electrolysis process, Chem. Eng. Sci. 54 (1999) 2501–2511.
[56] S.J. Paddison, The modeling of molecular structure and ion transport in sulfonic acid based ionomer membranes, J. New Mater. Electrochem. Syst. 4 (4) (2001) 197–207.
[57] K.T. Adjemian, S.J. Lee, S. Srinivasan, J. Benziger, A.B. Bocarsly, Silicon oxide Nafion composite membranes for proton-exchange membrane fuel cell operation at 80–140 °C, J. Electrochem. Soc. 149 (3) (2002) 256–261.
[58] K.T. Adjemian, S. Srinivasan, J. Benziger, A.B. Bocarsly, Investigation of PEMFC operation above 100 °C employing perfluorosulfonic acid silicon oxide composite membranes, J. Power Sources 109 (2) (2002) 356–364.
[59] P. Costamagna, C. Yang, A.B. Bocarsly, S. Srinivasan, Nafion 115/zirconium phosphate composite membranes for operation of PEMFCs above 100 °C, Electrochim. Acta 47 (2002) 1023–1033.